Pharmaceutical Research, Vol. 23, No. 8, August 2006 (© 2006)
DOI: 10.1007/s11095-006-9031-4

Research Paper

Kinetic Modeling of Nitric-Oxide-Associated Reaction Network

Teh-Min Hu,[1,4] William L. Hayton,[2] and Susan R. Mallery[3]

Received February 10, 2006; accepted April 7, 2006

Purpose. Nitric oxide and superoxide are the two important free radicals in the biological system. The coexistence of both free radicals in the physiological milieu gives rise to intricate oxidative and nitrosative reactions, which have been implicated in many physiological and/or pathophysiological conditions, such as vasodilatation and inflammation. It is difficult, if not impossible, to study the complexity of the nitric oxide/superoxide system using current experimental approaches. Computational modeling thus offers an alternative way for studying the problem.
Methods. In this present study, key reaction pathways related to the generation, reaction and scavenging of both nitric oxide and superoxide were integrated into a reaction network. The network dynamics was investigated by numerical simulations to a set of coupled differential equations and by dynamical analysis. Two specific questions pertaining to the reaction kinetics of the reactive chemical species in the nitric oxide/superoxide system were studied: (1) how does the system respond dynamically when the generation rate of nitric oxide and superoxide varies? (2) how would antioxidants such as glutathione modulate the system dynamics?
Results. While changing basal GSH levels does not alter the kinetics of nitric oxide, superoxide, and peroxynitrite, the kinetic profiles of N_2O_3, GSNO and GSH are sensitive to the variation of basal GSH levels. The kinetics of the potential nitrosative species, N_2O_3, is switch like, which is dependent on the level of GSH.
Conclusions. The model predicts that concurrent high nitric oxide and superoxide generation—such as in the inflammatory conditions—may result in nonlinear system dynamics, and glutathione may serve as a dynamic switch of N_2O_3 mediated nitrosation reaction.

KEY WORDS: antioxidants; glutathione; *in silico*; modeling and simulation; nitric oxide; superoxide.

INTRODUCTION

The free radical nitric oxide (NO) mediates a large number of physiological and pathophysiological processes. Despite more than a decade of intensive research, many aspects of NO physiological chemistry remain both paradoxical and controversial. At low concentrations (~nM), NO modulates normal physiological functions such as regulation of vascular tone and intracellular signaling via a direct interaction with its targets (1). However, high NO levels can induce cytotoxicity, presumably attributable to oxidative and nitrosative stresses (1). Elevated NO levels present at inflammatory sites provide the opportunity for NO to compete with superoxide dismutase (SOD) for reactions with superoxide (O_2^-), thereby generating the highly reactive and cytotoxic peroxynitrite ($ONOO^-$) molecule (2). Our previous study showed that low [SOD] stimulated—whereas high [SOD] attenuated—NO-mediated nitrosation reaction, and that glutathione (GSH) modulated the biphasic effect of SOD (3). The results suggest that the consequences of oxidative and nitrosative chemistry may depend heavily on a delicate balance among the processes that govern the formation and elimination of NO and O_2^-.

Because of the complex nature of NO and technical difficulties in studying its biological features, computational modeling has been used as an alternative tool for understanding diverse aspects of NO, which included (i) the biotransport of NO (4–8); (ii) kinetics related to the generation and reaction of NO (9–16); (iii) functions of NO in physiological and pathophysiological processes, such as neural signaling (17) and wound healing (18); (iv) mechanistic role of NO on the activation of soluble guanylyl cyclase (19). For example, mathematical modeling of NO diffusion predicted that NO is not a locally acting mediator, due to its rapid and wide spread diffusibility. Thus, one NO-producing cell can affect many hundred of its neighboring cells (20). Modeling approaches were also applied to examine the processes in the interaction of $ONOO^-$ with low-density lipoproteins (LDLs) in the plasma (12–14). The kinetic model predicted that

[1] School of Pharmacy, National Defense Medical Center, Taipei, Taiwan, Republic of China.
[2] Division of Pharmaceutics, College of Pharmacy, The Ohio State University, Columbus, Ohio 43210-1241, USA.
[3] Department of Oral and Maxillofacial Surgery and Pathology, College of Dentistry, The Ohio State University, Columbus, Ohio 43210-1241, USA.
[4] To whom correspondence should be addressed. (e-mail: tmhu@ndmctsgh.edu.tw)

plasma [$ONOO^-$] should be in nM range and $ONOO^-$ is a potential candidate for initiating peroxidation of LDLs (11). Once $ONOO^-$ is formed, antioxidants have little effect on the $ONOO^-$ level (12). Furthermore, a reaction/diffusion model was used to explore the movement of $ONOO^-$ into the LDL particle (13).

The formation of NO in the tissue is catalyzed by nitric oxide synthases (NOS), which are heme-containing enzymes. The expression of the different NOS isoforms is regulated by diverse mechanisms (21). While NOS1 [NOS I, neuronal NOS (nNOS)] and NOS3 [NOS III, endothelial NOS (eNOS)] are low-output, constitutive enzymes whose activities are regulated by Ca^{2+} and calmodulin, NOS2 [NOS II, inducible NOS (iNOS)] is a high-output enzyme, which after induction can produce a large amount of NO in a Ca^{2+}-independent fashion (21). Apparently, the amount of NO produced in tissues is a dynamic process that depends on which enzyme is involved, and where and when the enzyme is expressed.

In tissues, NO has an extremely short half-life, on the order of seconds (22). In addition to the high mutual reactivity between NO and O_2^- (23), NO also undergoes autooxidation with a rate that is dependent on the concentration of oxygen (22). Thus, both O_2 and O_2^- play an important role in the rapid scavenging of NO. The respective reaction intermediates, N_2O_3 and $ONOO^-$, for NO-O_2 and NO-O_2^- reactions were attributed to the indirect cytotoxic actions of NO (1). While N_2O_3 was believed to be a strong nitrosating agent towards targets, such as DNA and proteins, $ONOO^-$ is a potent oxidant and has been shown to react with a large number of biomolecules *in vitro*. The oxidative activity of $ONOO^-$ contributes substantially to tissue damage in inflammatory and infective diseases (1).

In this present study, key reaction pathways associated with NO-mediated nitrosative and oxidative chemistry were integrated into a reaction network. The dynamics of this network was then investigated. Two specific questions were examined: (i) what is the role of GSH in modulating nitrosative and oxidative species, such as N_2O_3 and $ONOO^-$? (ii) how does the system behave when the generation rate of NO and O_2^- varies?

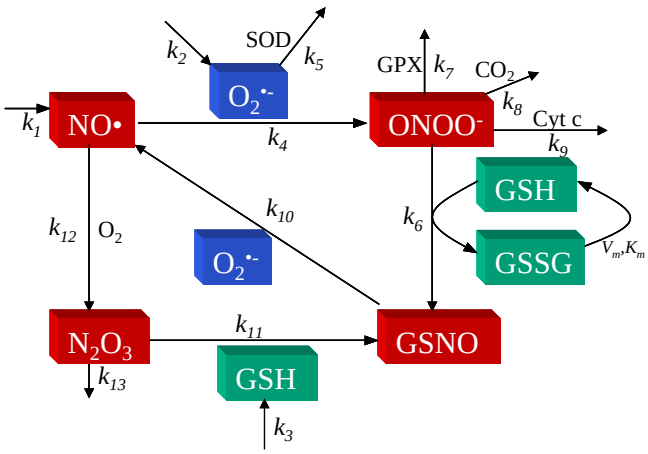

Fig. 1. The Model. SOD, superoxide dismutase; GPX, glutathione peroxidase; *cyt c*, cytochrome c; GSSG, oxidized glutathione.

Table I. The Rate Constants Used for the Simulation

Constant	Value	Reference
k_1	10^{-10}–10^{-5} Ms^{-1}	Vaughn *et al.* (15); Laurent *et al.* (16); Savill *et al.* (24)
k_2	10^{-8}–10^{-5} Ms^{-1}	Turner *et al.* (25); O'Donnell and Azzi (26)
k_3	varied	
k_4	6.7×10^9 $M^{-1}s^{-1}$	Huie and Padmaja (27)
k_5	2.4×10^9 $M^{-1}s^{-1}$	Fielden *et al.* (28)
k_6	1.35×10^3 $M^{-1}s^{-1}$	Koppenol *et al.* (29)
k_7	2×10^6 $M^{-1}s^{-1}$	Sies *et al.* (30)
k_8	5.8×10^4 $M^{-1}s^{-1}$	Denicola *et al.* (31)
k_9	2.5×10^4 $M^{-1}s^{-1}$	Thomson *et al.* (32)
k_{10}	6×10^8 $M^{-2}s^{-1}$	Jourd'heuil *et al.* (33)
k_{11}	6.6×10^7 $M^{-1}s^{-1}$	Keshive *et al.* (34)
k_{12}	6×10^6 $M^{-2}s^{-1}$	Wink *et al.* (35)
k_{13}	1.6×10^3 s^{-1}	Licht *et al.* (36)
V_m	3.2×10^{-4} Ms^{-1}	Antunes *et al.* (37)

MATERIALS AND METHODS

Model

Figure 1 integrates the reaction pathways related to NO and its reaction products, N_2O_3, $ONOO^-$ and nitrosoglutathione (GSNO). The concentrations of NO, N_2O_3, $ONOO^-$ and GSNO as well as the free radical O_2^- and antioxidant GSH were simulated. The general procedure was first to write a set of coupled differential equations based on the law of mass action. The differential equations were then solved simultaneously by numerical methods. Since the reaction kinetics of the integrative system was the main interest of this study, transport and diffusion processes were not included in the model.

Reaction Chemistry and Rate Constants

The NO production rates were estimated to be in the range from 1×10^{-10} to 1.6×10^{-8} M/s for adherent cells expressing iNOS (16). Using mathematical modeling, Vaughn *et al.* (15) predicted the rate of NO production by vascular endothelium of $\sim 10^{-5}$ M/s. In addition, the NO production rate by basal epidermal cell was estimated to be 1.7×10^{-7} M/s (24). Cultured keratinocyte cells (25) and fibroblasts (26) generated O_2^- at a rate of $\sim 10^{-6}$ M/s and $\sim 10^{-5}$ M/s, respectively. The rate constants were summarized in Table I (27–37). The rate equations for NO, O_2^-, $ONOO^-$, GSNO, N_2O_3, GSNO and GSH were:

$$\frac{d[NO]}{dt} = k_1 + k_{10}[GSNO]^2[O_2^-] - k_4[NO][O_2^-] - k_{12}[NO]^2[O_2] \quad (1)$$

$$\frac{d[O_2^-]}{dt} = k_2 - k_4[NO][O_2^-] - k_5[O_2^-][SOD] - k_{10}[GSNO]^2[O_2^-] \quad (2)$$

Table II. Parameter Values for the Simulation

Parameter	Value	Reference
$[O_2]$	35 μM	Antunes *et al.* (37)
$[CO_2]$	1–25 mM	Radi *et al.* (39)
[*cyt c*]	400 μM	Radi *et al.* (39)
[SOD]	1–10 μM	Beckman and Koppenol (23)
[GPX]	5.8 μM	Antunes *et al.* (37)
K_m	50 μM	Antunes *et al.* (37)
[GSH]	1–10 mM	Griffith (40)

$$\frac{d[ONOO^-]}{dt} = k_4[NO][O_2^-] - k_6[ONOO^-][GSH] - (k_7[GPX] + k_8[CO_2] + k_9[cyt\ c])[ONOO^-] \quad (3)$$

$$\frac{d[GSNO]}{dt} = k_6[ONOO^-][GSH] + k_{11}[N_2O_3][GSH] - k_{10}[GSNO]^2[O_2^-] \quad (4)$$

$$\frac{d[N_2O_3]}{dt} = k_{12}[NO]^2[O_2] - k_{11}[N_2O_3][GSH] - k_{13}[N_2O_3] \quad (5)$$

$$\frac{d[GSH]}{dt} = k_3 - (k_6[ONOO^-][GSH] + k_{11}[N_2O_3][GSH]) + \frac{V_m[GSSG]}{K_m + [GSSG]} \quad (6)$$

$$[GSSG] = [GSH]_0 - [GSH] - [GSNO] \quad (7)$$

Numerical Simulations

Numerical simulations of the model Eqs. (1), (2), (3), (4), (5), (6), (7) were carried out using NDSolve in Mathematica 4.0 [Wolfram Research, Champagne, IL]. NDSolve can solve *stiff* differential equations using Backward Differentiation Formulas (or Gear Formulas). The approximation error in NDSolve is controlled by two built-in functions of Mathematica, AccuracyGoal and Precision-

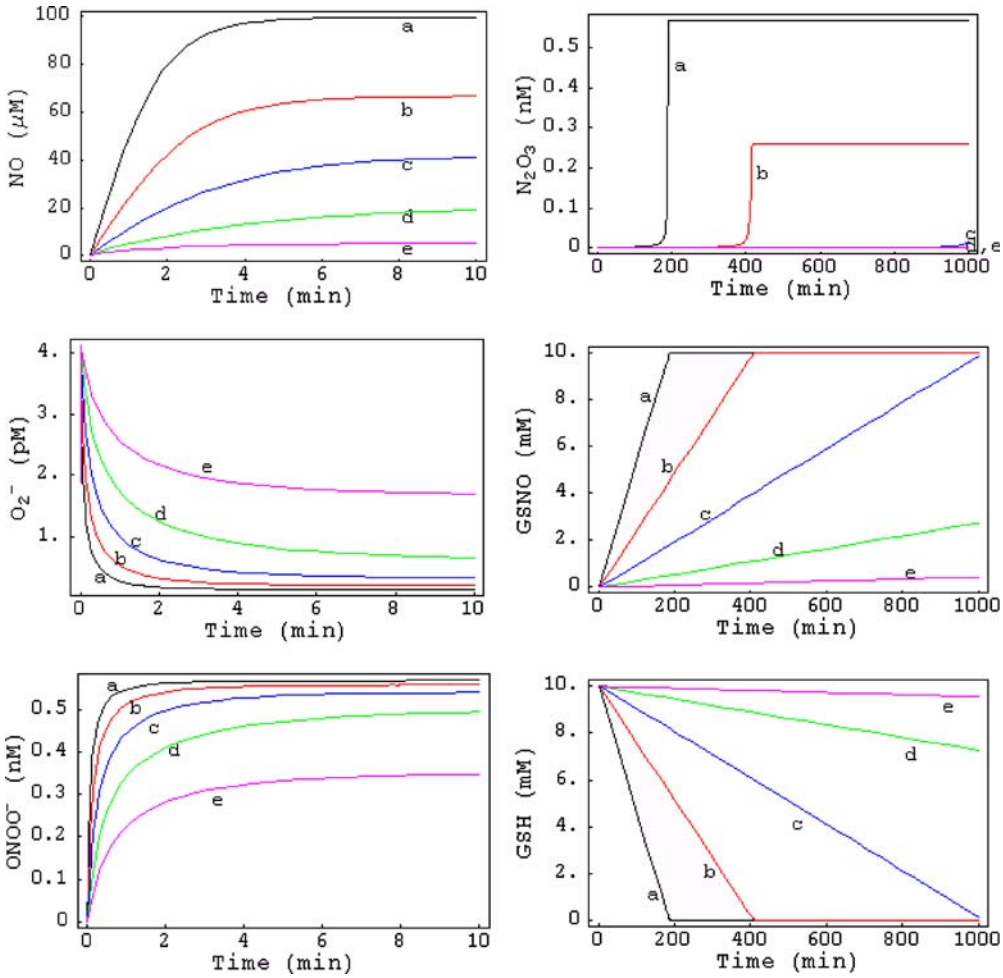

Fig. 2. Kinetic profiles of various species in the simulated scenarios with $[GSH]_{basal}$ = 10 mM. Scenarios: (a) $k_1 = k_2$; (b) $k_1 = 0.5\ k_2$; (c) $k_1 = 0.25\ k_2$; (d) $k_1 = 0.125\ k_2$; (e) $k_1 = 0.0625\ k_2$, where $k_2 = 1 \times 10^{-7}$ M/s for all scenarios.

Goal, which specify absolute and relative error, respectively. NDSolve attempts to calculate a solution, $y(x)$, with error less than $10^{-a} + |y(x)|10^{-p}$, where a and p are positive integers that represent the settings for AccuracyGoal and PrecisionGoal, respectively (38). For this study, the error was set to no more than 10^{-15}.

The model consists of seven dependent variables, which are the chemical species to be simulated. The rate constants k_1 to k_3 were subjected to variation, while k_4 to k_{13} were fixed as constant parameters. Other constants are V_m, K_m, $[O_2]$, $[CO_2]$, [*cyt c*], [SOD], [GPX]. The values for these constants are shown in Table II (23,37,39,40).

RESULTS

The Model

Figure 1 is a simplified schematic to show the interrelationship among various reacting species. The exact reaction mechanism for each reaction is not shown in Fig. 1, but is considered in formulating the rate law of each reacting species. For example, the reaction between NO and O_2 was shown to be second order with respect to NO and first order to O_2, and overall a third order reaction. The third-order rate constant (k_{12} in Fig. 1) has been reported in (35), as indicated in Table I.

In this simulation study, the rate constants k_1 through k_3 were subject to variation while the rate constants k_4 through k_{13} were fixed. The reason is two-fold. First, k_1, k_2, and k_3 represent the rate constant for the generation of NO, O_2^-, and GSH, respectively, which, according to the two major study questions of this study, were the key parameters to manipulate. Second, while k_1 through k_3 are associated with cellular biochemistry and physiology and are variable in different cells or conditions, the other parameters are experimentally measured and reported rate constants of chemical reactions, which were directly obtained from the literature, as indicated in Table I.

Kinetic Profiles

Figures 2, 3 and 4 show the concentration-time profiles for NO, O_2^-, $ONOO^-$, N_2O_3, GSNO and GSH in 3 separate simulations where the initial GSH level was varied. For each simulation, five scenarios were considered. Each scenario had a two-fold difference in the generation rate of NO—i.e., two-fold difference in k_1. The results indicate that changing basal

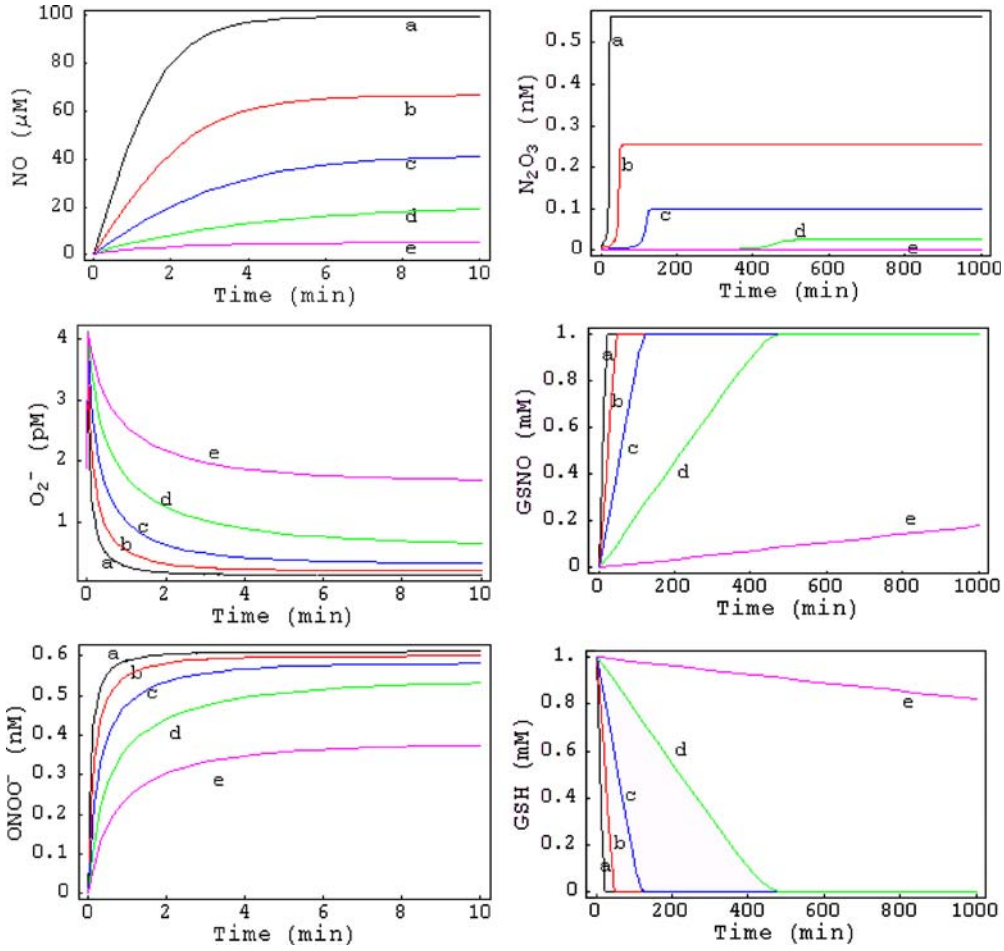

Fig. 3. Kinetic profiles of various species in the simulated scenarios with $[GSH]_{basal}$ = 1 mM. Scenarios: (a) $k_1 = k_2$; (b) $k_1 = 0.5\ k_2$; (c) $k_1 = 0.25\ k_2$; (d) $k_1 = 0.125\ k_2$; (e) $k_1 = 0.0625\ k_2$, where $k_2 = 1 \times 10^{-7}$ M/s for all scenarios.

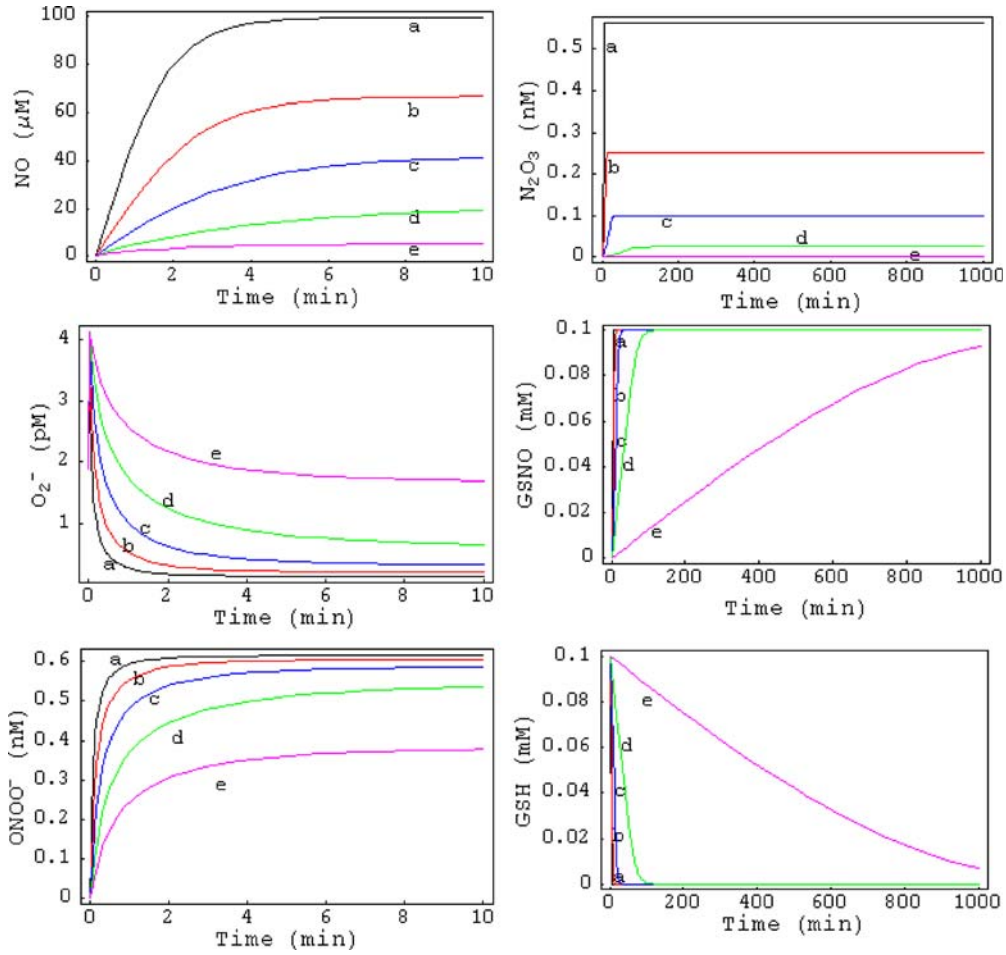

Fig. 4. Kinetic profiles of various species in the simulated scenarios with $[GSH]_{basal}$ = 0.1 mM. Scenarios: (a) $k_1 = k_2$; (b) $k_1 = 0.5\ k_2$; (c) $k_1 = 0.25\ k_2$; (d) $k_1 = 0.125\ k_2$; (e) $k_1 = 0.0625\ k_2$, where $k_2 = 1 \times 10^{-7}$ M/s for all scenarios.

GSH levels does not alter the kinetics of NO, O_2^-, and $ONOO^-$, with the steady-state concentrations being in the micromolar, picomolar and nanomolar range, respectively (left panels, Figs. 2, 3 and 4). The kinetics of the three species reaches steady state within 10 min. The steady-state concentrations decrease (NO and $ONOO^-$) or increase (O_2^-) corresponding to the reduction of k_1.

The kinetic profiles of N_2O_3, GSNO and GSH are sensitive to the variation of basal GSH levels (right panels, Figs. 2, 3 and 4). The profiles are consistent in a sense that [GSNO] continuously increases at the expense of GSH and N_2O_3. As a result, [GSH] is depleted and the time for a complete depletion depends on the basal level of GSH (Figs. 2, 3 and 4) and the input rate of NO (individual curves in each figure). It is interesting to note that GSH and GSNO follow zero-order kinetics before GSH is exhausted, which disobeys second-order rate equations for these two species. This discrepancy will be discussed later.

GSH as a Dynamic Switch

As indicated in the model (Fig. 1), the continuous generation of NO contributes to the formation of N_2O_3, a potential nitrosating agent. Strikingly, N_2O_3 is maintained at an extremely low level due to the presence of GSH (Fig. 2). An instantaneous elevation of $[N_2O_3]$ is apparent when [GSH] approaches a critical value (Fig. 2). The kinetic profiles are therefore step-like. Moreover, the slower the NO-generation rate is, the longer for this phenomenon to be initiated, and the lower is the new steady-state $[N_2O_3]$. When the basal [GSH] is reduced to 1 and 0.1 mM (Figs. 3 and 4), GSH is depleted much more quickly, followed by much earlier switching of $[N_2O_3]$ than it is at 10 mM. To further explore the switch-like phenomenon, simulations with a zero-order replenish of GSH were performed. The result shows that the system responds in a switch-like fashion (Fig. 5). $[N_2O_3]$ is sensitive to the perturbation and is reduced to a new steady state immediately. Overall, the data suggest that GSH acts as a dynamic switch in the reaction network.

Nonlinear Dynamics at High NO and O_2^- Input Rates

To study the system behavior at high NO and O_2^- input rates, simulations were conducted by setting k_1 and k_2 100 times higher, while keeping k_1/k_2 ratios and other parameters the same as in Fig. 2. The results show that the dynamic patterns in Fig. 6 significantly deviate from those in Fig. 2. The concentrations of NO are below 5 μM for all simulations

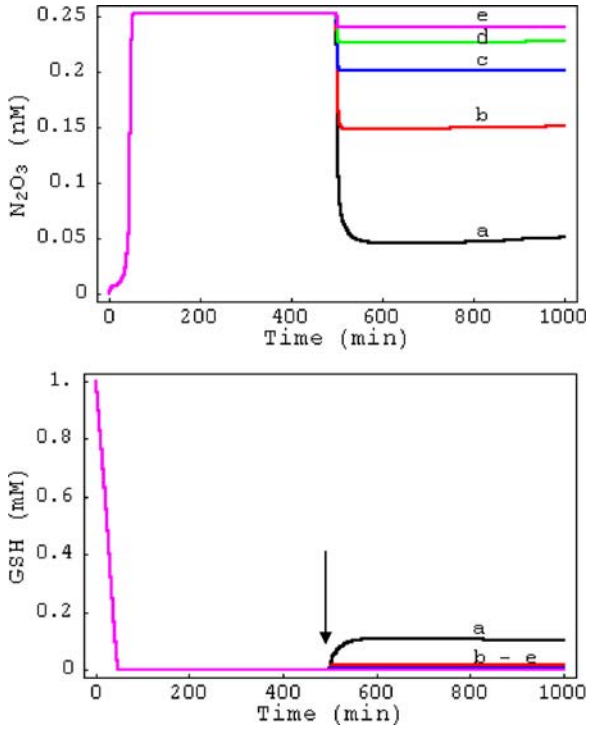

Fig. 5. Effect of various GSH input rates on the concentration-time profiles of N_2O_3 and GSH, where initial [GSH] = 1 mM. *Arrow*: start of zero-order GSH input (k_3). k_2 = 6 μM/min; k_1 = 0.5 k_2; k_3 = (a) 20 μM/min; (b) 10 μM/min; (c) 5 μM/min; (d) 2.5 μM/min; (e) 1.25 μM/min.

with k_1/k_2 ratios in the range of 0.0625–0.5, but at equal NO and O_2^- input rate, [NO] reaches to 70 μM at steady state (Fig. 6). Compared with Fig. 2, [NO] is relatively lower while $[O_2^-]$ is higher in all scenarios in Fig. 6. The result suggests that an increase in NO production couldn't guarantee an increase in [NO] as long as the input of O_2^- is not fixed. Another interesting result, as compared with Fig. 2, is the elevation of $[ONOO^-]$ in Fig. 6, which suggests that the system is more efficient in terms of the generation of $ONOO^-$. Finally, the kinetics of N_2O_3, GSNO and GSH in the right panel of Fig. 6 coincides with the role and the kinetics of NO.

Phase Portraits

A phase-portrait approach (41) was used to account for the kinetic behavior illustrated in Fig. 6. To construct a phase portrait, the relationship between $\frac{d[NO]}{dt}$ and [NO] was plotted according to Eq. (1), assuming that the contribution of GSNO to the kinetics of NO is negligible under the simulation conditions. Hence, Eq. (1) becomes

$$\frac{d[NO]}{dt} = k_1 - k_4[NO]\left[O_2^-\right] - k_{12}[NO]^2[O_2]. \quad (8)$$

The steady-state O_2^- concentration with the same assumption is

$$\left[O_2^-\right] \approx \frac{k_2}{k_4[NO] + k_5[SOD]}. \quad (9)$$

Substituting Eq. (9) into Eq. (8), Eq. (1) becomes

$$\frac{d[NO]}{dt} = k_1 - \frac{k_2 k_4[NO]}{k_4[NO] + k_5[SOD]} - k_{12}[NO]^2[O_2]. \quad (10)$$

Since k_4, k_5, k_{12}, [SOD] and $[O_2]$ were known parameters, by varying the ratio k_1/k_2 and plotting the data $\left(\frac{d[NO]}{dt} = f(NO)\right.$ *versus* $\left.[NO]\right)$, a set of curves was obtained (Fig. 7A). The *x*-axis intersect implies $\frac{d[NO]}{dt} = 0$, with the corresponding value on *x*-axis being the steady-state concentration of NO, $[NO]_{ss}$. By plotting $[NO]_{ss}$ *versus* k_1/k_2, a nonlinear curve was obtained. This curve captures the essence of nonlinearity in NO kinetics in Fig. 6; if $k_1 \leq 0.5k_2$, $[NO]_{ss}$ is low and insensitive to the variations in k_1; nevertheless, $[NO]_{ss}$ increases disproportionately as k_1 increases beyond 0.5 k_2. For the purpose of comparison, Fig. 8 shows a scenario where the dynamics is approximately linear.

DISCUSSION

Using mathematical modeling, this study examined two questions related to the reaction kinetics of nitrogen oxide species (NO_x) in an integrative dynamic system: (i) what is the role of GSH in modulating nitrosative and oxidative species, such as N_2O_3 and $ONOO^-$? (ii) how does the system behave when the generation rate of NO and O_2^- varies? It is difficult to study these types of questions using experimental approaches, since it may require simultaneous measurements of multiple short-lived species at extremely low concentrations, in complex physiological matrices. Nevertheless, one can gain a reasonable picture of the behavior of an *in vivo* system by using a modeling approach to integrate the knowledge about individual elements (reactions) of the system. The underlying rationale was that the behavior of a complex system usually is not determined by an additive process.

Glutathione (GSH), the major low-molecular-weight thiol compound in the cell, is best known for its role as a superoxide scavenger in mediating cellular redox reactions (42). Since cellular GSH levels are as high as 10 mM and GSH reacts with $ONOO^-$ and N_2O_3 in aqueous media, it was suggested that GSH is a scavenger for reactive NO_x as well (43). Moreover, the S-nitrosation product of GSH—S-nitrosoglutathione (GSNO)—was considered as a possible carrier molecule for NO (44). GSH was shown to diminish the NO-mediated nitrosation reaction. It also modulated the biphasic dose-response relationship for the effect of SOD on NO-mediated nitrosation (3). Since [GSH] ranges from several hundred μM (extracellular) to about 10 mM (intracellular), the effect of GSH on the kinetics of NO_x was simulated with initial [GSH] = 0.1, 1 and 10 mM, respectively. That GSH does not affect the kinetic profiles of NO and $ONOO^-$ (Figs. 2, 3 and 4) reflects the fact that in the model GSH does not react with NO directly, and that the GSH pathway is not the predominant route for the elimination of $ONOO^-$. Besides GSH, $ONOO^-$ also reacts with a wide variety of biomolecules. In this study, the reactions of $ONOO^-$ with CO_2, cytochrome c (*cyt c*) and glutathione peroxidase (GPX) were only included because of the relative importance of these reactions (Fig. 1). $ONOO^-$ reacts rap-

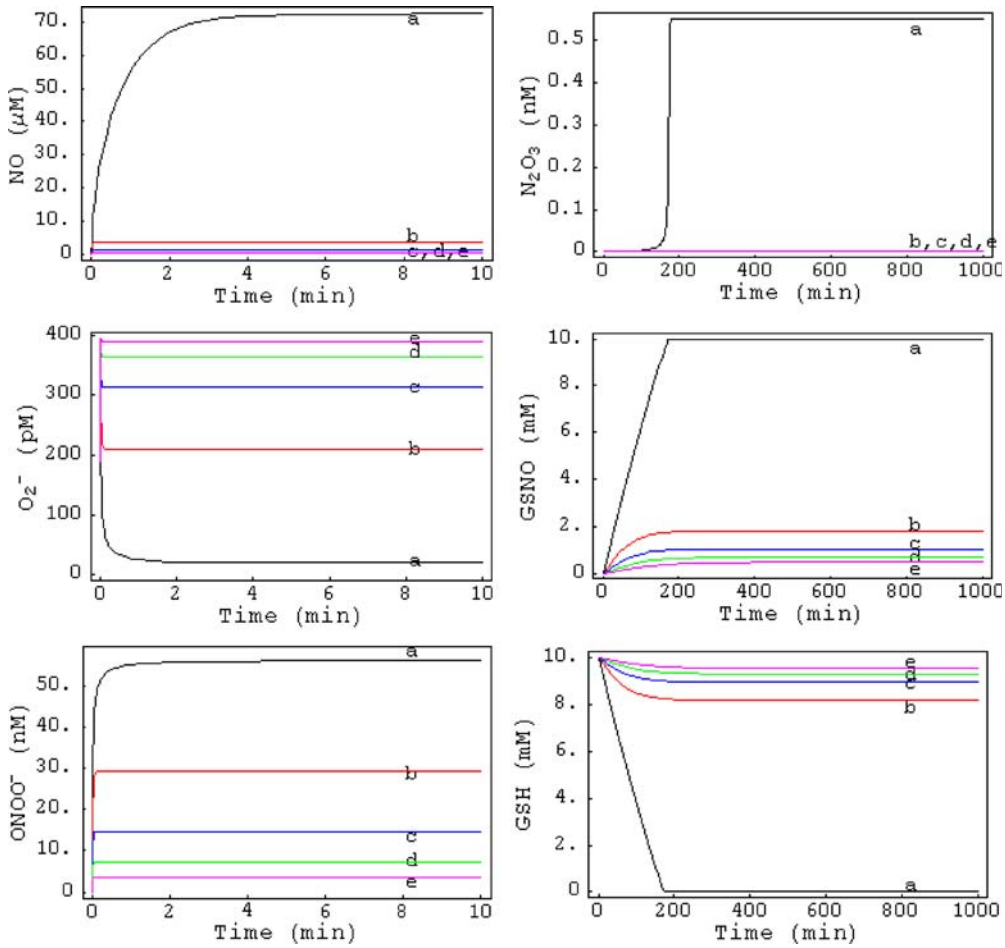

Fig. 6. Kinetic profiles of various species for simulated scenarios with high superoxide generation rate. Scenarios: (a) $k_1 = k_2$; (b) $k_1 = 0.5\ k_2$; (c) $k_1 = 0.25\ k_2$; (d) $k_1 = 0.125\ k_2$; (e) $k_1 = 0.0625\ k_2$. $[GSH]_{basal} = 10$ mM, $k_2 = 1 \times 10^{-5}$ M/s for all scenarios.

idly with CO_2 ($k = 5.8 \times 10^4\ M^{-1}s^{-1}$) to generate nitrosoperoxycarbonate adduct, which decomposes to NO_3^- and CO_2 in the absence of other reactive molecules (31,45).

$$ONOO^- + CO_2 \rightarrow ONO_2CO_2^- \tag{11}$$

$$ONO_2CO_2^- \rightarrow NO_3^- + CO_2 \tag{12}$$

Since CO_2/bicarbonate/carbonate is an important buffering system *in vivo* and the concentrations of CO_2 (1.3 mM in plasma) and bicarbonate (12 mM in intracellular fluid and 25–30 mM in plasma) are high, the reaction between $ONOO^-$ and CO_2 could be the major route of $ONOO^-$ disappearance *in vivo* (45,46). Although the rate constants for the reactions between $ONOO^-$ and GPX ($2 \times 10^6\ M^{-1}s^{-1}$) (30)—and between $ONOO^-$ and *cyt c* ($2 \times 10^5\ M^{-1}s^{-1}$) (32)—are relatively higher than that for the $ONOO^-$-CO_2 reaction, the contribution of GPX and cyt c in eliminating $ONOO^-$ could be less significant due to their relatively lower concentrations in biological fluids (Table II). The rate constant for the reaction between $ONOO^-$ and GSH is $1.35 \times 10^3\ M^{-1}s^{-1}$ (29), which is the smallest compared with those of the abovementioned reactions. Therefore, GSH will be far less effective than CO_2 in modulating $ONOO^-$ levels in the physiological environment, where GSH is less abundant, e.g., blood plasma. In contrast, GSH may become important inside the cells because of its high intracellular concentration (10 mM). The reason that $[ONOO^-]$ in Fig. 2 is comparable to that in Figs. 2 and 3 is because the reaction rate of $ONOO^-$ with 1 mM CO_2 is still at least four-fold larger than that with GSH, even though [GSH] is as high as 10 mM.

Zero-order kinetics was observed for GSH and GSNO, which disobeyed the rate laws for both species. Since $ONOO^-$ and N_2O_3 are the two molecules responsible for the depletion of GSH and the accumulation of GSNO in the model, the discrepancy could be resolved when the kinetics of $ONOO^-$ and N_2O_3 was examined. While $[ONOO^-]$ reaches steady state within 10 min, $[N_2O_3]$ is kept at nearly constant and extremely low levels before GSH is completely depleted (Fig. 2). Therefore, $\frac{d[ONOO^-]}{dt}$ and $\frac{d[N_2O_3]}{dt}$ are approximately zero in the early period. From Eqs. (3) and (5), one immediately obtains:

$$\begin{aligned} k_6[ONOO^-][GSH] &= k_4[NO][O_2^-] \\ &\quad - (k_7[GPX] + k_8[CO_2] + k_9[cyt\,c])[ONOO^-] \end{aligned} \tag{13}$$

$$k_{11}[N_2O_3][GSH] = k_{12}[NO]^2[O_2] - k_{13}[N_2O_3] \tag{14}$$

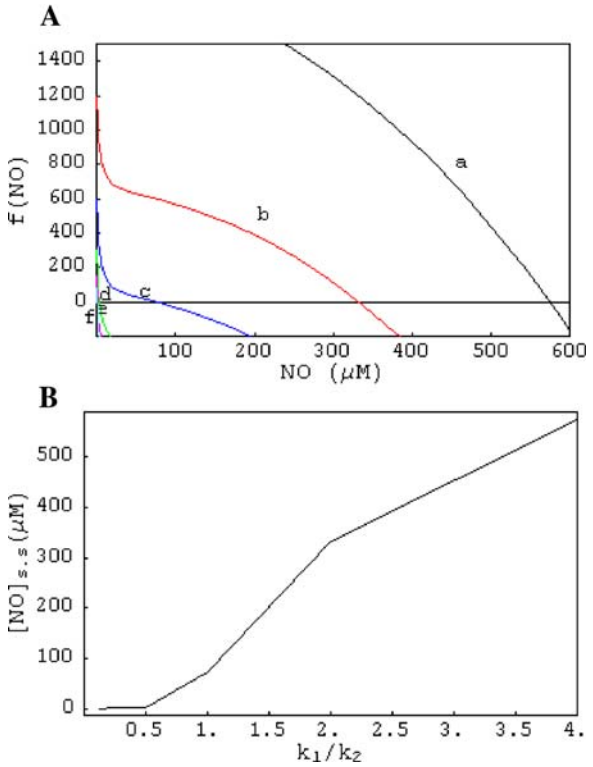

Fig. 7. (A) Phase portraits of [NO] (B) $[NO]_{ss}$ *versus* k_1/k_2. $k_2 = 1 \times 10^{-5}$ M/s; k_1/k_2 = (a) 4; (b) 2; (c) 1; (d) 0.5; (e) 0.25; (f) 0.125.

Since [NO] and $[O_2^-]$ also reaches steady states very quickly (Fig. 2), and [GPX], $[CO_2]$, $[O_2]$ and [cyt c] are constants, it implies that the term $k_6[ONOO^-][GSH] + k_{11}[N_2O_3][GSH]$ in Eqs. (4) and (6) is close to a constant and, therefore, the elimination of GSH and the formation of GSNO follows zero-order kinetics.

The current study proposes that GSH can act as a dynamic switch that controls the concentration of N_2O_3, which is an intriguing phenomenon from both kinetic and biological standpoints. By closely examining Eq. (5) and the rate constants (Table I), one finds that $k_{11}[GSH] \gg k_{13}$ when [GSH] = 1–10 mM. Accordingly, the elimination of N_2O_3 is controlled by GSH at high levels. Under this circumstance, the hydrolysis of N_2O_3—corresponding to the rate constant k_{13}—becomes a redundant elimination pathway that contributes insignificantly to the whole process. The concentration of N_2O_3 remains quite low due to the presence of sufficiently high levels of GSH (Fig. 2 or Fig. 3). However, the once redundant pathway becomes increasingly important as GSH approaches a depletion point at which the alternate elimination pathway takes over and a new steady state switches on. The nearly instantaneous occurrence of the new steady-state can be attributed to the first-order rate constant k_{13} (Table I), which corresponds to a half-life as short as 0.4 ms.

From a biological standpoint, a sudden elevation of a reactive NO_x in a physiological system could be catastrophic. N-nitrosation may result in the deamination of DNA bases (39). Furthermore, S-nitrosation of proteins was attributed to the inhibition of some enzymes, such as glyceraldehydes-3-phosphate dehydrogenase (47) and the DNA repair enzyme O^6-methylguanine-DNA-methyltransferase (48). Abrupt changes in S-nitrosation status may also disrupt redox-based signaling transduction pathways (49). GSH, therefore, may play an important role in modulating NO_x-mediated cytotoxicity. For example, the NO donor DEA/NO only caused a modest toxicity in Chinese hamster V79 cells (43). However, the toxicity was dramatically increased when GSH was depleted in these cells. Recently, cellular GSH status was linked to the differential iNOS regulation in hepatocytes and inflammatory cells (50). While iNOS induction in hepatocytes *in vivo* and *in vitro* was dependent on the intracellular GSH status and correlated with NF-κB binding, GSH-depletion had no effect on the expression of iNOS in inflammatory cells (50).

Phase portraits are widely used to characterize the qualitative behavior of a dynamical system, especially a nonlinear one (41). For a simple one-dimensional system, $dx/dt = f(x)$, a graph of $f(x)$—i.e., a plot of dx/dt *vs.* x—is considered as the phase portrait of the system. One of the advantages of using phase portrait approach is to immediately show how many steady-state solutions or fixed points the system has. A fixed point x^* in the phase portrait is defined as $x(t) = x^*$ such that $f(x^*) = 0$, i.e., the steady state solution ($x(t) = x^*$ such that $dx/dt = 0$) of the system (41). Once the fixed point is located, the curvature of the phase portrait (the shape of $f(x)$) can give us some idea as to how the steady state or equilibrium is reached. In this study, phase portraits were constructed based on a simplified rate equation for NO, Eq. (10), to further verify the numerical results, especially for the concentration profiles of NO. By setting $d[NO]/dt = f(NO)$ = the right hand side of Eq. (10), and plotting f(NO), a phase portrait for the NO system is obtained. For example, In Fig. 7A, each line (a through e) represents the phase diagram of each simulated

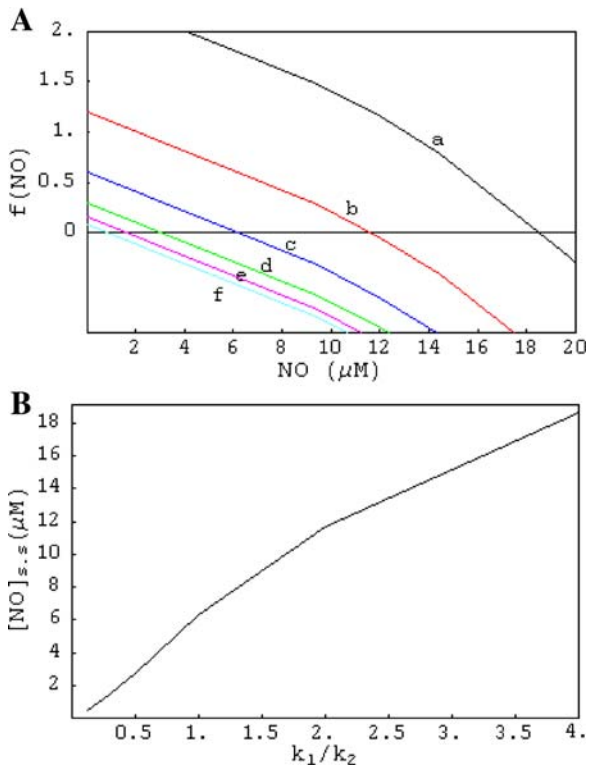

Fig. 8. (A) Phase portraits of [NO] (B) $[NO]_{ss}$ *versus* k_1/k_2. $k_2 = 1 \times 10^{-8}$ M/s; k_1/k_2 = (a) 4; (b) 2; (c) 1; (d) 0. 5; (e) 0.25; (f) 0.125.

condition with a fixed k_1/k_2 value. There is one fixed point (i.e., the x intercept) in each line, which corresponds to the steady state concentration of NO. The corresponding $[NO]_{ss}$ was plotted against the k_1/k_2 ratio in Fig. 7B to show the dependence of $[NO]_{ss}$ on the relative input rate of NO and O_2^-, which unequivocally manifests the nonlinear NO kinetics observed in Fig. 6.

The present study describes an *in silico* dynamic modeling approach to study the complex system of reactive nitrogen and oxygen species. The proposed modeling and simulation method provides a systematic way to study the NO associated reaction system and may have implication in many pathophysiological conditions. Nevertheless, because of the unavoidable simplistic nature of the model and uncertainties in the values of parameters used, the simulation results should be interpreted with caution. The major concern with the model is the applicability of the simulation results to the realistic situations, such as in cells. The modeling presented here assumes that the proposed reaction network is within a closed, homogeneous system where the transport and diffusion of the reacting molecules are neglected, which might be reasonable, given the reactivity of the reactive species studied. The model further assumes that constant inputs of both reactive free radicals, NO and O_2^-, are maintained for several hours (e.g., during inflammation), during which the effects of cell volume and cellular bioregulatory responses toward the change of system dynamics are possibly ignored. We would like to point out that the simulation results presented here should be viewed as qualitative or "proof of principle" only. Any new information about the proposed reaction network may warrant further modification of the model. This present modeling study, therefore, is only a first step towards a better understanding of a complex system involving reactive nitrogen and oxygen species.

CONCLUSIONS

Kinetic modeling was used to explore the reaction network associated with the free radicals NO and O_2^-. Numerical simulations provided two testable predictions: (i) GSH might modulate the nitrosation reaction in a switch-like fashion; (ii) concurrently high NO and O_2^- generation might result in nonlinear dynamics of nitrogen oxide species.

REFERENCES

1. K. M. Miranda, M. G. Espey, D. Jourd'heuil, M. B. Grisham, J. M. Fukuto, M. Feelisch, and D. A. Wink. The chemical biology of nitric oxide. In L. J. Ignarro (ed.), *Nitric oxide: Biology and Pathobiology*, Academic, San Diego, 2000, pp. 41–55.
2. R. P. Patel, J. McAndrew, H. Sellak, C. R. White, H. Jo, B. A. Freeman, and V. M. Darley-Usmar. Biological aspects of reactive nitrogen species. *Biochim. Biophys. Acta* **1411**:385–400 (1999).
3. T. M. Hu, W. L. Hayton, M. A. Morse, and S. R. Mallery. Dynamic and biphasic modulation of nitrosation reaction by superoxide dismutases. *Biochem. Biophys. Res. Commun.* **295**:1125–1134 (2002).
4. D. G. Buerk. Can we model nitric oxide biotransport? A survey of mathematical models for a simple diatomic molecule with surprisingly complex biological activities. *Annu. Rev. Biomed. Eng.* **3**:109–143 (2001).
5. J. R. Lancaster Jr. Simulation of the diffusion and reaction of endogenously produced nitric oxide. *Proc. Natl. Acad. Sci. USA* **91**:8137–8141 (1994).
6. J. R. Lancaster Jr. A tutorial on the diffusibility and reactivity of free nitric oxide. *Nitric Oxide* **1**:18–30 (1997).
7. M. W. Vaughn, L. Kuo, and J. C. Liao. Effective diffusion distance of nitric oxide in the microcirculation. *Am. J. Physiol.* **274**:H1705–H1714 (1998).
8. H. Y. Shin and S. C. George. Microscopic modeling of NO and S-nitrosoglutathione kinetics and transport in human airways. *J. Appl. Physiol.* **90**:777–788 (2001).
9. B. Chen and W. M. Deen. Analysis of the effects of cell spacing and liquid depth on nitric oxide and its oxidation products in cell cultures. *Chem. Res. Toxicol.* **14**:135–147 (2001).
10. S. P. Goss, N. Hogg, and B. Kalyanaraman. The effect of nitric oxide release rates on the oxidation of human low density lipoprotein. *J. Biol. Chem.* **272**:21647–21653 (1997).
11. W. D. Stanbro. A kinetic model of the system: tyrosyl radical-nitrogen oxide-superoxide ion. *J. Theor. Biol.* **197**:557–567 (1999).
12. W. D. Stanbro. Modeling the interaction of peroxynitrite with low-density lipoproteins. III. The role of antioxidants. *J. Theor. Biol.* **205**:473–482 (2000).
13. W. D. Stanbro. Modeling the interaction of peroxynitrite with low-density lipoproteins. II. Reaction/diffusion model of peroxynitrite in low-density lipoprotein particles. *J. Theor. Biol.* **205**: 465–471 (2000).
14. W. D. Stanbro. Modeling the interaction of peroxynitrite with low-density lipoproteins. I. Plasma levels of peroxynitrite. *J. Theor. Biol.* **205**:457–464 (2000).
15. M. W. Vaughn, L. Kuo, and J. C. Liao. Estimation of nitric oxide production and reaction rates in tissue by use of a mathematical model. *Am. J. Physiol.* **274**:H2163–H2176 (1998).
16. M. Laurent, M. Lepoivre, and J. P. Tenu. Kinetic modelling of the nitric oxide gradient generated *in vitro* by adherent cells expressing inducible nitric oxide synthase. *Biochem. J.* **314**(Pt 1): 109–113 (1996).
17. A. Philippides, P. Husbands, and M. O'Shea. Four-dimensional neuronal signaling by nitric oxide: a computational analysis. *J. Neurosci.* **20**:1199–1207 (2000).
18. C. A. Cobbold and J. A. Sherratt. Mathematical modelling of nitric oxide activity in wound healing can explain keloid and hypertrophic scarring. *J. Theor. Biol.* **204**:257–288 (2000).
19. D. P. Ballou, Y. Zhao, P. E. Brandish, and M. A. Marletta. Revisiting the kinetics of nitric oxide (NO) binding to soluble guanylate cyclase: the simple NO-binding model is incorrect. *Proc. Natl. Acad. Sci. USA* **99**:12097–12101 (2002).
20. J. R. Lancaster Jr. The physical properties of nitric oxide: determinants of the dynamics of NO in tissue. In L. J. Ignarro (ed.), *Nitric Oxide: Biology and Pathobiology*, Academic, San Diego, 2000, pp. 209–224.
21. H. Kleinert, J.-P. Boissel, P. M. Schwarz, and U. Forstermann. Regulation of the expression of nitric oxide synthase isoforms. In L. J. Ignarro (ed.), *Nitric Oxide: Biology and Pathobiology*, Academic, San Diego, 2000, pp. 105–128.
22. D. D. Thomas, X. Liu, S. P. Kantrow, and J. R. Lancaster Jr. The biological lifetime of nitric oxide: implications for the perivascular dynamics of NO and O2. *Proc. Natl. Acad. Sci. USA* **98**:355–360 (2001).
23. J. S. Beckman and W. H. Koppenol. Nitric oxide, superoxide, and peroxynitrite: the good, the bad, and ugly. *Am. J. Physiol.* **271**:C1424–C1437 (1996).
24. N. J. Savill, R. Weller, and J. A. Sherratt. Mathematical modelling of nitric oxide regulation of rete peg formation in psoriasis. *J. Theor. Biol.* **214**:1–16 (2002).
25. C. P. Turner, A. M. Toye, and O. T. Jones. Keratinocyte superoxide generation. *Free Radic. Biol. Med.* **24**:401–407 (1998).
26. V. B. O'Donnell and A. Azzi. High rates of extracellular superoxide generation by cultured human fibroblasts: involvement of a lipid-metabolizing enzyme. *Biochem. J.* **318**(Pt 3): 805–812 (1996).
27. R. E. Huie and S. Padmaja. The reaction of no with superoxide. *Free Radic. Res. Commun.* **18**:195–199 (1993).
28. E. M. Fielden, P. B. Roberts, R. C. Bray, D. J. Lowe, G. N. Mautner, G. Rotilio, and L. Calabrese. Mechanism of action of superoxide dismutase from pulse radiolysis and electron paramagnetic resonance. Evidence that only half the active sites function in catalysis. *Biochem. J.* **139**:49–60 (1974).

29. W. H. Koppenol, J. J. Moreno, W. A. Pryor, H. Ischiropoulos, and J. S. Beckman. Peroxynitrite, a cloaked oxidant formed by nitric oxide and superoxide. *Chem. Res. Toxicol.* **5**:834–842 (1992).
30. H. Sies, V. S. Sharov, L. O. Klotz, and K. Briviba. Glutathione peroxidase protects against peroxynitrite-mediated oxidations. A new function for selenoproteins as peroxynitrite reductase. *J. Biol. Chem.* **272**:27812–27817 (1997).
31. A. Denicola, B. A. Freeman, M. Trujillo, and R. Radi. Peroxynitrite reaction with carbon dioxide/bicarbonate: kinetics and influence on peroxynitrite-mediated oxidations. *Arch. Biochem. Biophys.* **333**:49–58 (1996).
32. L. Thomson, M. Trujillo, R. Telleri, and R. Radi. Kinetics of cytochrome c2+ oxidation by peroxynitrite: implications for superoxide measurements in nitric oxide-producing biological systems. *Arch. Biochem. Biophys.* **319**:491–497 (1995).
33. D. Jourd'heuil, C. T. Mai, F. S. Laroux, D. A. Wink, and M. B. Grisham. The reaction of S-nitrosoglutathione with superoxide. *Biochem. Biophys. Res. Commun.* **246**:525–530 (1998).
34. M. Keshive, S. Singh, J. S. Wishnok, S. R. Tannenbaum, and W. M. Deen. Kinetics of S-nitrosation of thiols in nitric oxide solutions. *Chem. Res. Toxicol.* **9**:988–993 (1996).
35. D. A. Wink, J. F. Darbyshire, R. W. Nims, J. E. Saavedra, and P. C. Ford. Reactions of the bioregulatory agent nitric oxide in oxygenated aqueous media: determination of the kinetics for oxidation and nitrosation by intermediates generated in the NO/O2 reaction. *Chem. Res. Toxicol.* **6**:23–27 (1993).
36. W. R. Licht, S. R. Tannenbaum, and W. M. Deen. Use of ascorbic acid to inhibit nitrosation: kinetic and mass transfer considerations for an *in vitro* system. *Carcinogenesis* **9**:365–372 (1988).
37. F. Antunes, A. Salvador, H. S. Marinho, R. Alves, and R. E. Pinto. Lipid peroxidation in mitochondrial inner membranes. I. An integrative kinetic model. *Free Radic. Biol. Med.* **21**:917–943 (1996).
38. K. R. Coombes, B. R. Hunt, R. L. Lipsman, J. E. Osborn, and G. J. Stuck. *Differential Equations with Mathematica*, Wiley, New York, 1998.
39. R. Radi, A. Denicola, B. Alvarez, G. Ferrer-Sueta, and H. Rubbo. The biological chemistry of peroxynitrite. In L. J. Ignarro (ed.), *Nitric Oxide: Biology and Pathobiology*, Academic, San Diego, 2000, pp. 57–82.
40. O. W. Griffith. Biologic and pharmacologic regulation of mammalian glutathione synthesis. *Free Radic. Biol. Med.* **27**:922–935 (1999).
41. S. H. Strogatz. *Nonlinear Dynamics and Chaos*. Addison-Wesley, Reading, Massachusetts, 1994.
42. H. Sies. Glutathione and its role in cellular functions. *Free Radic. Biol. Med.* **27**:916–921 (1999).
43. D. A. Wink, R. W. Nims, J. F. Darbyshire, D. Christodoulou, I. Hanbauer, G. W. Cox, F. Laval, J. Laval, J. A. Cook, and M. C. Krishna. Reaction kinetics for nitrosation of cysteine and glutathione in aerobic nitric oxide solutions at neutral pH. Insights into the fate and physiological effects of intermediates generated in the NO/O2 reaction. *Chem. Res. Toxicol.* **7**:519–525 (1994).
44. B. Gaston. Nitric oxide and thiol groups. *Biochim. Biophys. Acta* **1411**:323–333 (1999).
45. S. Pfeiffer, B. Mayer, and B. Hemmens. Nitric oxide: chemical puzzles posed by a biological messenger. *Angew. Chem. Int. Ed.* **38**:1714–1731 (1999).
46. M. P. Murphy, M. A. Packer, J. L. Scarlett, and S. W. Martin. Peroxynitrite: a biologically significant oxidant. *Gen. Pharmacol.* **31**:179–186 (1998).
47. L. Molina y Vedia, B. McDonald, B. Reep, B. Brune, M. Di Silvio, T. R. Billiar, and E. G. Lapetina. Nitric oxide-induced S-nitrosylation of glyceraldehyde-3-phosphate dehydrogenase inhibits enzymatic activity and increases endogenous ADP-ribosylation. *J. Biol. Chem.* **267**:24929–24932 (1992).
48. F. Laval and D. A. Wink. Inhibition by nitric oxide of the repair protein, O6-methylguanine-DNA-methyltransferase. *Carcinogenesis* **15**:443–447 (1994).
49. J. S. Stamler, S. Lamas, and F. C. Fang. Nitrosylation: the prototypic redox-based signaling mechanism. *Cell* **106**:675–683 (2001).
50. T. A. Vos, H. Van Goor, L. Tuyt, A. De Jager-Krikken, R. Leuvenink, F. Kuipers, P. L. Jansen, and H. Moshage. Expression of inducible nitric oxide synthase in endotoxemic rat hepatocytes is dependent on the cellular glutathione status. *Hepatology* **29**:421–426 (1999).